Aalborg Universitet

Thermal Cycling Overview of Multi-Megawatt Two-Level Wind Power Converter at Full Grid Code Operation

Zhou, Dao; Lau, Mogens ; Blaabjerg, Frede; Tonnes, Michael

[Link to publication from Aalborg University](#)

Paper

Thermal Cycling Overview of Multi-Megawatt Two-Level Wind Power Converter at Full Grid Code Operation

Dao Zhou[*a]   Non-member,   Frede Blaabjerg[*]   Non-member
Mogens Lau[**]   Non-member,   Michael Tonnes[**]   Non-member

In this paper, two promising multi-megawatt wind turbines equipped with a doubly-fed induction generator-based partial-scale and a permanent magnet synchronous generator-based full-scale two-level power converter are designed and compared. Simulations of the two configurations with respect to loss distribution and junction temperature variation for the power device over the entire wind speed range are presented and analyzed both for normal operation and operation with various specific grid codes. It is concluded that in both partial-scale and full-scale power converters, the most thermal stressed power device in the generator-side converter will have a higher mean junction temperature and also junction temperature variation compared to the grid-side converter at the rated wind speed, and the thermal performance of the generator-side converter in the partial-scale power converter becomes crucial around the synchronous operating point and needs to be considered carefully. Moreover, reactive power injection directed by the grid codes will affect the thermal profile of the power semiconductors, especially at lower wind speeds.

Keywords: two-level wind power converter, power losses, thermal cycling, grid codes

1. Introduction

Over last two decades, the wind power industry has expanded greatly. Meanwhile, the European countries commit themselves to realize 20% of the total electricity production through wind energy by 2020[1]. In response to the steady growth of the wind power demand, several significant trends emerge: The power level of a single wind turbine is increasing from dozens of kW up to 10 MW in order to obtain lower cost per kWh as well as increasing the power density of the system. The location of wind farm is moving from onshore to offshore to reduce environment impact due to land limitation and richer wind energy resources. Moreover, due to the higher cost after failure, the lifetime of wind power generation system is in turn prolonged to 20–25 years, which requires for a more reliable and durable wind power system[2][3].

Unfortunately, the investigation of wind turbines in north Germany in time period of 1993–2006 indicates that the increasing power rating of the wind turbine will have a higher risk of failure[4]. Considering the failure rate and down time distribution within a wind turbine system, as shown in Fig. 1, although the gearbox and generator have the longest down time, it is the power converters that in this survey dominate the failures[5]–[7].

Power semiconductors are nowadays playing a key role in power electronic system, and more and more efforts are devoted to the reliability characteristic. As different stressors

distribution shown in Fig. 2, temperature cycling is regarded as having the most significant impact[8]. It is widely accepted that the thermal profile of the power semiconductor is an important indicator of lifetime[9]–[19] and it has an influence on the lifetime. The power cycle numbers to failure[20] is relevant to the junction temperature fluctuation ΔT_j as well as

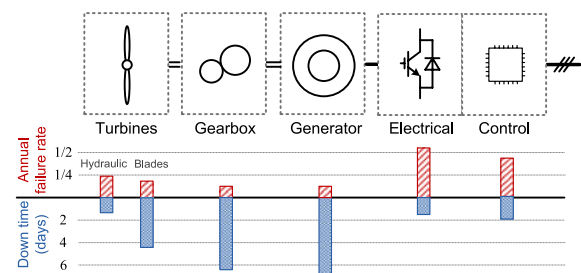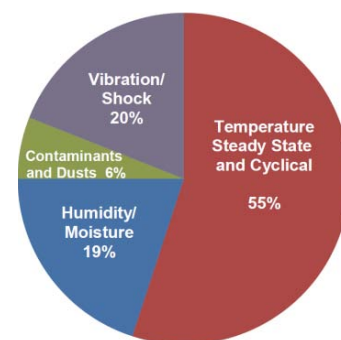Fig. 1. Distribution of failure rate and down time for different parts in a wind turbine system[5]

Fig. 2. Stressors distribution in a power electronics system[8]

a) Correspondence to: Dao Zhou. E-mail: zda@et.aau.dk
* Department of Energy Technology, Aalborg University
  Pontoppindanstraede 101, Aalborg, DK-9220, Denmark
** Danfoss Silicon Power GmbH
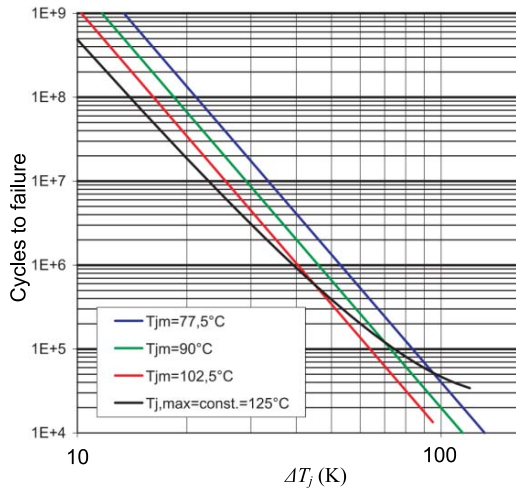 Husumer Strasse 251, Flensburg, D-24941, Germany

Fig. 3. Typical example of cycles to failure v.s. ΔT_j and T_{jm} in IGBT module [20]

(a) Wind turbine system with partial-scale power converter

(b) Wind turbine system with full-scale power converter

Fig. 4. Typical configurations for wind turbine system
DFIG: Doubly-Fed Induction Generator,
SG: Synchronous Generator, IG: Induction Generator

the mean junction temperature T_{jm} of power semiconductor, which is illustrated in Fig. 3.

The scope of this paper is to analyze and simulate the thermal cycling of multi-MW partial-scale and full-scale power converter through an electro-thermal approach, and compare the power semiconductor junction temperature mean value and variation in order to do an initial reliability assessment. First, the typical configurations for variable speed wind turbine system will be introduced. Then, the basic design of the wind power converter as well as the relevant grid codes will be described. Finally, loss distribution and thermal analysis will be presented and compared in respect to the power device performance for the two different configurations.

2. Typical Wind Turbine Configurations

Due to the extensive and well-established knowledge, as well as the simpler circuit structure and fewer components, the two-level back-to-back voltage source converter is the most attractive solution in the commercial market of wind turbines [3]. The utilization of the power electronics in wind turbine system can be further divided into two categories, namely: a wind turbine system with partial-scale power converter and a wind turbine system with full-scale power converter, which both are illustrated in Fig. 4.

2.1 Wind Turbine System with Partial-scale Power Converter   A popular wind turbine configuration, normally based on the Doubly-Fed Induction Generator (DFIG), is to employ a power converter rated approximately 30% of the nominal generator power in order to handle around 30% of the slip power. The topology is shown in Fig. 4(a).

The power converter is connected to the rotor through slip-rings and makes the rotor current as well as rotor speed under control, while the stator is linked to the grid without any decoupling. If the generator operates in super-synchronous mode, the electrical power is delivered through both the rotor and stator. If the generator is running sub-synchronously, the electrical power is only delivered into the grid from the stator.

The fraction of slip power through the converter makes this concept attractive from an economical point of view. However, the main drawbacks lie in the use of slip rings, and also an additional crowbar is needed to protect the generator-side
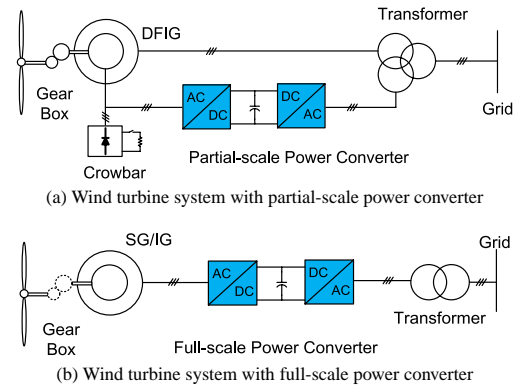
converter under grid faults [21].

2.2 Wind Turbine System with Full-scale Power Converter   As shown in Fig. 4(b), another full-scale power converter configuration equipped with Synchronous Generator (SG) or Induction Generator (IG) is considered as a promising technology for multi-MW wind turbine system.

The generator stator winding is connected to the grid through a full-scale power converter, which performs the reactive power compensation and also a smooth grid connection for the entire operating speed. Some variable speed wind turbine system may become gearless by introducing the multi-pole generator.

The elimination of the slip rings, simpler gearbox and full power controllability during the grid faults are the main advantages. However, in order to satisfy the power rating, the widely used approach nowadays is to implement several converter modules or power devices in parallel, which of course are challenging the complexity and reliability of the whole wind turbine system.

3. Operation of the Wind Turbine System

As shown in Fig. 4, the partial-scale power converter is normally connected to a DFIG, while the full-scale power converter equips a Permanent Magnet Synchronous Generator (PMSG). For simplicity, these two configurations are named the DFIG system and the PMSG system, respectively. In order to evaluate and compare the thermal performance for the above two systems, a mathematical model and a simulation platform will first be established.

3.1 Wind Turbine Model   A 2 MW wind turbine system is used for the case studies. The energy transferred from the kinetic wind power to mechanical power can be expressed as [22]

$$P_G = \frac{1}{2}\rho\pi R^2 C_p(\lambda,\beta)v_w^3 \cdots\cdots\cdots\cdots\cdots\cdots\cdots (1)$$

where ρ denotes the air density (kg/m³), R denotes the radius of turbine blade (m), and v_w denotes the wind speed (m/s). Depending on the blade pitch angle β and tip speed ratio λ, the power coefficient C_p represents the aerodynamical transfer efficiency, whose maximum value can be obtained under optimal tip speed ratio.

The parameters of the wind turbine are summarized in Table 1 [23]. Also, the relationship between the wind speed,

Table 1. Parameters for 2 MW wind turbine (DFIG/PMSG)

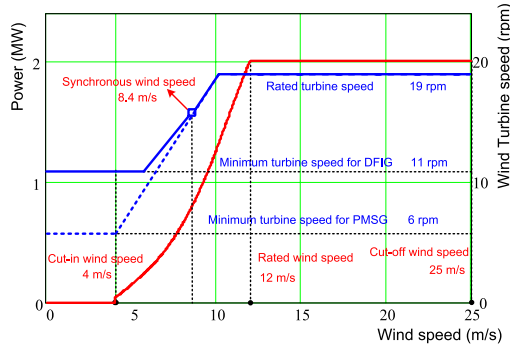| Wind turbine parameters	
Rated power P_G [MW]	2
Blade radius R [m]	41.3
Cut-in wind speed v_{wcut_in} [m/s]	4
Rated wind speed v_{w_rate} [m/s]	12
Cut-off wind speed v_{wcut_off} [m/s]	25
Optimal tip speed ratio λ_{opt}	8.1
Maximum power coefficient C_{pmax}	0.383
Rated turbine speed n_{rot_rate} [rpm]	19
Minimum turbine speed n_{rot_min} [rpm]	11/6

Fig. 5. Relationship between wind speed, turbine rotor speed and output power for the two different 2 MW systems
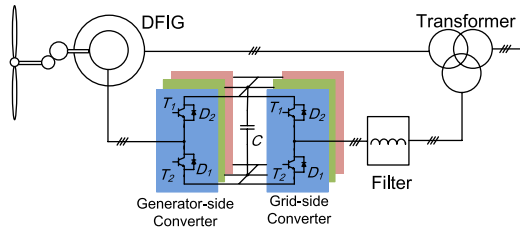

Fig. 6. Two-level back-to-back converter of a DFIG system

turbine rotor speed and produced output power is shown in Fig. 5.

3.2 Power Device Selection in Two Different Systems
Fig. 6 shows a DFIG system that consists of a generator, a partial-scale power converter, a filter and a transformer. Since the stator is directly connected to low-voltage grid, the DC-link voltage is set as low as possible seen from the power device lifetime point of view. Moreover, the filter inductance is designed to limit the current ripple within 0.25 p.u. [24].

Due to the DC capacitor decoupling, the power converter can be divided into the generator-side converter and the grid-side converter. Each of the control schemes can be designed separately.

For the generator-side converter, one of the control objectives focuses on transferring produced active power to the grid. The other purpose is to provide the excitation current for the DFIG. The grid-side converter will keep the DC-link voltage fixed and meet the reactive power demand according to the grid codes. Furthermore, Space-Vector Pulse Width Modulation (SVPWM) is used to generate the switching signals for the power semiconductors in both converters.
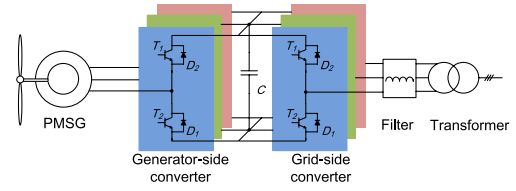

Fig. 7. Two-level back-to-back converter of a PMSG system

Table 2. 2 MW generator data for DFIG and PMSG [26][27]

	DFIG	PMSG
Rated wind speed $v_{w\ rate}$ [m/s]	12	
Rated turbine speed $n_{rot\ rate}$ [rpm]	19	
Number of pole pairs p	2	102
Gear ratio	94.7	/
Rated shaft speed n_s [rpm]	1800	19
Fundamental frequency at rated power f_e [Hz]	10	32.3
Stator leakage inductance L_{ls} [mH]	0.038	0.276
Magnetizing inductance L_m [mH]	2.91	
Rotor leakage inductance L_{lr} [mH]	0.064	/
Stator/rotor turns ratio n	0.369	/

The typical PMSG system equipped with a full-scale power converter is shown in Fig. 7, which consists of a generator-side converter and a grid-side converter. Compared to the DFIG system, the current through both converters will be much higher under the same power rating of the wind turbines, which means the selection of power devices in the two configurations will be quite different in order to realize similar power device loading. Nevertheless, the design method of the DC-link voltage and the filter inductance in the PMSG system can be referred to as the DFIG system.

Considering the control scheme of the generator-side converter, the current through the stator of the generator should be controlled to adjust the rotating speed for maximum power. On the contrary, the reference of the d-axis current is set to zero for minimum power loss [25].

For the grid–side converter, the outer DC-link voltage and inner current closed loop have the ability to perform a fast active power control performance and to control the injected or absorbed reactive power, which are almost the same as the grid-side converter in the DFIG system. As mentioned before, the produced power through the power converter semiconductors is quite different in the DFIG and the PMSG system. Consequently, it is important to select suitable power devices for both systems in order to obtain a fair comparison for the thermal loading.

It is assumed that the two systems are using the wind turbine system as illustrated in Table 1. The typical parameters for the generators are summarized in Table 2. The PMSG system is a direct-drive for multi-pole structure, while for the DFIG system, a gearbox is still required as a multi-pole low-speed DFIG is not technically feasible.

Table 3.　Two-level back-to-back power converter data

	DFIG	PMSG
Rated active power P_C [kW]	400	2000
DC-link voltage U_{dc} [V$_{dc}$]	1050	
Switching frequency f_s [kHz]	2	
Grid-side Converter		
Rated voltage [V$_{rms}$]	704	704
Rated current [A$_{rms}$]	328	1641
Filter inductance [mH]	0.50	0.15
Power modules in each arm	1 kA/1.7 kV, single	1 kA/1.7 kV, 4 in parallel
Generator-side Converter		
Rated voltage [V$_{rms}$]	374	554
Rated current [A$_{rms}$]	618	2085
Power modules in each arm	1 kA/1.7 kV, 2 in parallel	1 kA/1.7 kV, 4 in parallel

The most important data for the two-level back-to-back converter are listed in Table 3. The switching frequency in both configurations and both converters are set to 2 kHz. The rated active power in the DFIG system is much smaller than the PMSG system, as only slip power flows through both converters. Based on the active power, together with the rated converter voltage output, the current in the converter needs to be calculated.

It is noted that in the DFIG system the rated current in the more unequal, while the situation is more equal in the PMSG system.

Furthermore, a parallel structure of multiple power components is a more used solution for multi-MW wind turbines today. Consequently, a common 1.7 kV/1 kA power device is selected. A single module in the grid-side converter and two paralleled modules in the generator-side converter are the solutions for the DFIG system, and four paralleled modules in both converters for the PMSG system are selected.

3.3　Grid Codes　　Power system operators are challenged by the increasing wind power penetration level to maintain the stability and reliability of the power system. Consequently, grid codes are issued and updated by transmission system operators of the different countries [28].

Reactive power control in the power system is considered as an important aspect in normal operation. As a large number of wind farms are continuously being installed in remote area of the power transmission system, the weak connections demand the ability of reactive power supply in order to support the voltage regulation [29].

For instance, the German code has imposed additional specifications concerning the minimum active/reactive power requirement for offshore wind power application as shown in Fig. 8, within a range of +/−5% around nominal voltage.
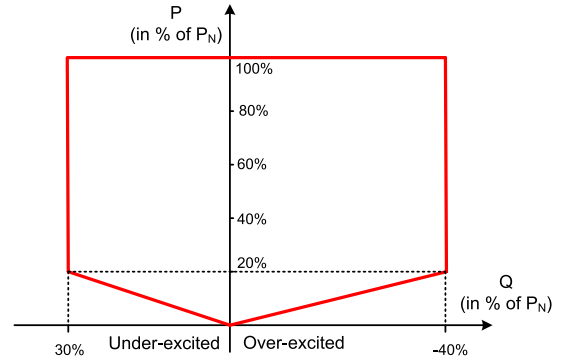
Fig. 8.　Offshore wind turbine requirement of active and reactive power defined by E.on-Netz [30]

4.　Power Loss Distribution of the Systems

4.1　Power Loss Model　　The power losses in the back-to-back converter consist of the generator-side converter loss and the grid-side converter loss. They are mainly divided into the switching losses and the conduction losses [31]. Since no unbalance is taken into account in this paper, it is possible to consider the behavior of half of one leg in both power converters due to the symmetrical characteristic and the fixed DC-link voltage.

No matter what the current direction is, the switching losses in each switching period always contain one turn-on loss E_{on}, one turn-off loss E_{off} in the IGBT, and one diode recovery loss E_{rr}. E_{on}, E_{off} and E_{rr} are almost proportional to the DC-link voltage, thus the formula for switching loss in each power device P_{sw} can be expressed as:

$$P_{sw} = f_e \frac{U_{dc}}{U_{dc}^*} \sum_{n=1}^{N} \left[E_{on}(|i_a(n)|) + E_{off}(|i_a(n)|) + E_{rr}(|i_a(n)|) \right]$$

$$\cdots\cdots\cdots\cdots\cdots\cdots (2)$$

where f_e denotes the fundamental frequency of output current, U_{dc}^* denotes the tested DC-link voltage, N denotes the total cycle numbers in each fundamental frequency, E_{on}, E_{off} and E_{rr} denote the switching loss energy in each switching period when the switching current equals to the phase current $|i_a(n)|$. E_{on}, E_{off}, E_{rr} and U_{dc}^* can typically be directly acquired from the power device datasheets.

The conduction losses mainly lie in the IGBT and the freewheeling diode. The conduction power loss in each power device P_{con} can be calculated as:

$$P_{con} = f_e \sum_{n=1}^{N} \left[v_{CE}(|i_a(n)|) \cdot |i_a(n)| \cdot T_1(n) \right.$$
$$\left. + v_F(|i_a(n)|) \cdot |i_a(n)| \cdot (T_s - T_1(n)) \right] \cdots\cdots (3)$$

where v_{CE} denotes the collector-emitter saturation voltage drop of the IGBT, v_F denotes the forward on-state voltage drop of the freewheeling diode, $T_1(n)$ denotes the conduction time of the IGBT during n^{th} switching period, which in line with the modulation strategies and the phase angle between phase current and phase voltage. T_s denotes the switching period.

4.2　Power Loss Distribution under Normal Operation　　Simulation of the power loss can be realized based on
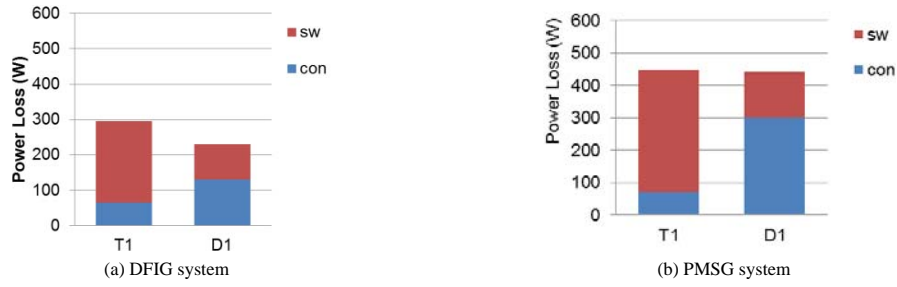
Fig. 9.　Loss distribution in generator-side converter for each power module (wind speed: 12 m/s).
Note: sw and con are switching losses and conduction losses, respectively
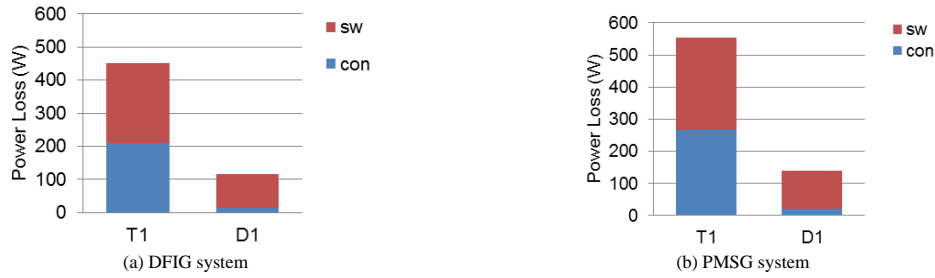

Fig. 10.　Loss distribution in grid-side converter for each power module (wind speed: 12 m/s).
Note: sw and con are switching losses and conduction losses, respectively

PLECS block in Simulink [32]. The simulation settings correspond to the design parameters shown in Table 2 and Table 3. In addition, the simulation circuit runs at rated wind speed under normal grid condition and the power factor is set to unity. Fig. 9 and Fig. 10 indicate the loss distribution of each power semiconductor under the DFIG and the PMSG systems in terms of the generator-side converter and the grid-side converter, respectively. The name of the power semiconductors can be found in Fig. 6 and Fig. 7.

Comparing the back-to-back power converter in both systems, the power losses dissipated in the generator-side converter are more equal. It is because the turn-on and turn-off loss of IGBT are higher than the recovery loss of freewheeling diode for the same current, from (2) the switching loss in the diode is always smaller. The conduction loss is mainly related to the power direction. At rated active power, the generator-side converter is operating as a rectifier, and therefore more conduction losses are seen in the freewheeling diode. On the contrary, the grid-side converter is operating as an inverter, where most of the conduction losses are dissipated in the IGBT, which results in an unequal loading.

For the DFIG and the PMSG systems, the power loss dissipated in the PMSG system is larger. The reason is that as summarized in Table 3, the current through each power semiconductor is higher.

In order to investigate the loss behavior in different operation modes, several wind speeds are chosen with slip values from −0.3 to 0.2 in the DFIG system and the parameters are shown in Table 4. It is noted that the wind speed at 8.4 m/s is regarded as the synchronous operating point as it is seen in Fig. 5 and also in Table 2.

The power loss in the generator-side converter at different wind speed is shown in Fig. 11. In order to avoid the extremely unbalanced power device loading at synchronous operating point, a small turbine speed hysteresis is introduced for minimum rotor frequency 1 Hz in the DFIG system [33].

Table 4.　Parameters for converters at different wind speed (DFIG/PMSG)

Wind speed [m/s]	Generator power [MW]	Wind turbine speed [rpm]	Slip	Fundamental frequency of output current [Hz]
5.9	0.26	11/10.1	0.3/0	15/17.2
6.8	0.39	12.7/12.0	0.2/0	10/20.4
7.6	0.55	14.2/13.7	0.1/0	5/23.3
8.4	0.74	15.8/15.4	0.02/0	0/26.2
9.2	0.98	17.2/17.1	−0.1/0	5/29.1
10.1	1.29	19/19	−0.2/0	10/32.3
12	2	19/19	−0.2/0	10/32.3
25	2	19/19	−0.2/0	10/32.3

The loss distribution of the IGBT and diode are illustrated in Fig. 11(a). In the super-synchronous mode, the power loss increases with larger wind speed, and the growth rate is relatively slower since the larger slip, which will decrease the converter current. Regarding the conduction loss, it is noted that the conduction loss in the diode is dominating. However, in the sub-synchronous mode, the conduction loss in the IGBT is dominating. For the PMSG system, as shown in Fig. 11(b), the power loss increases with the wind speed consecutively.

The power loss in the grid-side converter at different wind speed is shown in Fig. 12. For the DFIG system, the lowest power loss appears in the synchronous operating point due to the fact that no active power flow exist and only the switching ripple current affects, while the highest one appears at rated wind power. Furthermore, the IGBT suffers more loss in super-synchronous mode and the diode suffers more loss in sub-synchronous mode.
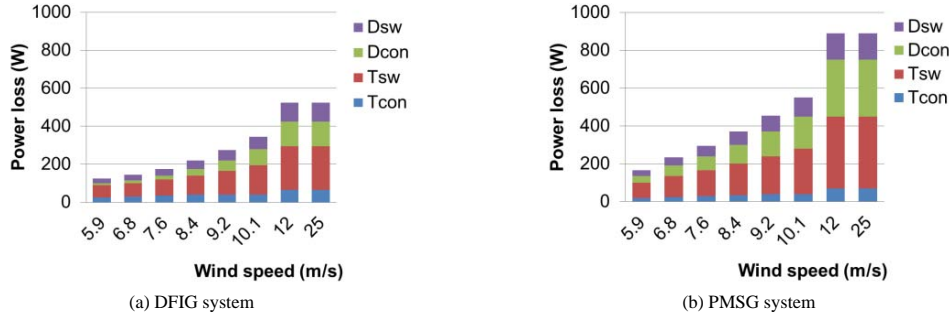
(a) DFIG system   (b) PMSG system

Fig. 11. Power loss of each power module vs. wind speed (generator-side converter)

(a) DFIG system   (b) PMSG system
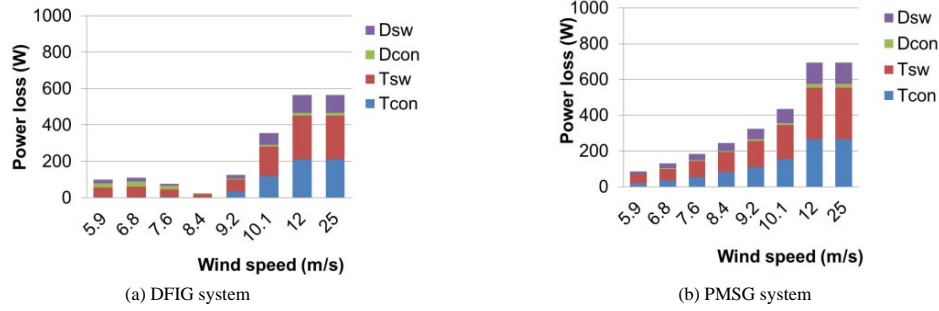
Fig. 12. Power loss of each power module v.s. wind speed (grid-side converter)

(a) Generator-side converter in the DFIG system   (b) Grid-side converter in the PMSG system
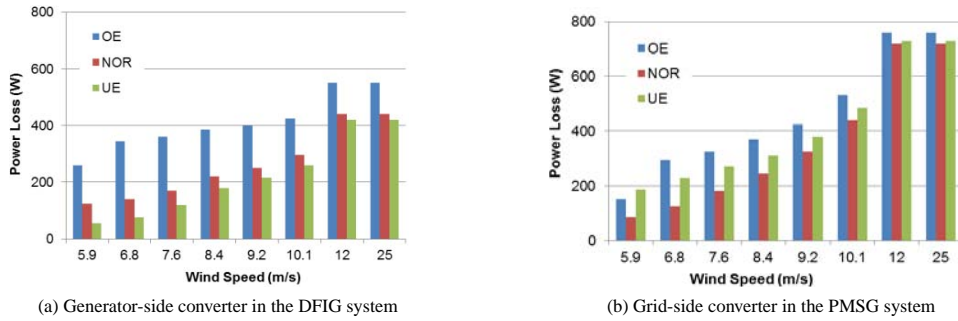
Fig. 13. Power loss profile of different system considering grid codes.
Note: OE, NOR and UE indicate over-excited, normal and under-excited reactive power

For the PMSG system, the power loss increases with the wind speed consecutively.

4.3 Power Loss Distribution Considering Grid Codes

If the German grid codes as shown in Fig. 8 are taken further into account, additional power loss will be introduced by reactive power injection. In the DFIG system, because of the winding ratio of the induction generator, higher current amplitude and larger power angle shift will be induced in the grid-side converter than in the generator-side converter, which means the reactive power compensated from the generator-side converter is a better choice [34]. For the PMSG system, the reactive power compensation can only be injected into the grid-side converter.

Therefore, the power loss profile is illustrated in Fig. 13 in terms of under-excited reactive power, normal operation and over-excited reactive power. For the DFIG system, it is noted that, due to the excitation energy for the induction generator is supplied by the grid code, the under-excited reactive power will relieve the power loss in the power device, while over-excited reactive power will make the DFIG system more stressed. For the PMSG system, no excitation

energy is required for the PMSG. Consequently, both the over-excited and under-excited reactive power will increase the power loss.

5. Thermal Analysis of the Systems

5.1 Thermal Model   As the thermal performance of the power devices are closely related to the reliability and the cost of the whole power converter system, a comparison of the thermal cycling of the DFIG and the PMSG systems will be investigated.

In order to describe the thermal behavior of the power semiconductors, an appropriate thermal model needs to be developed. The thermal models of single IGBT and the free-wheeling diode are shown in Fig. 14, and share the same design idea as discussed in [35][36], the thermal resistance R_{th} will determine the steady-state mean junction temperature, and along with the thermal capacitance (function of time constant τ) will determine the junction temperature fluctuation.

The thermal impedance from the junction to case $Z_{(j-c)}$ is modeled as a four-layer Foster RC network as depicted in Fig. 15, whose parameters are collected from the datasheet of

the power device. The case-to-heatsink thermal impedance is modeled as a simple thermal resistor, neglecting the much higher thermal capacitance due to the less significant dynamic behavior of the junction temperature and also obtain a faster thermal simulation. Meanwhile the heatsink-to-ambient resistance is considered small compared to the thermal resistance in the MW power converter. Furthermore, the ambient temperature is set to 50°C.

5.2 Thermal Cycling under Normal Operation The simulation results of the junction temperature in each power
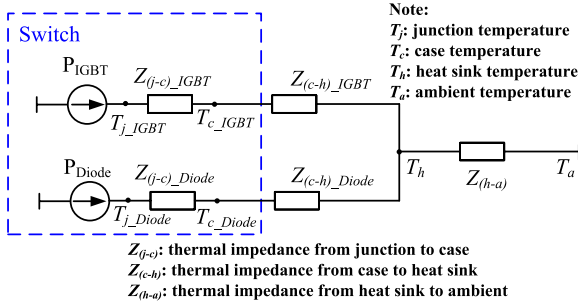

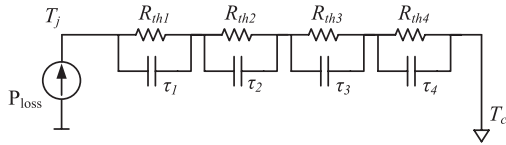Fig. 14. Thermal model of the power module

Fig. 15. RC Foster network of thermal impedance from junction to case of the power semiconductor devices

semiconductor of the generator-side converter under the DFIG and the PMSG systems are shown in Fig. 16 in which the converters run at rated power and in steady-state operation. It can be seen that the mean temperature of the diode is higher than the IGBT's in both the DFIG and the PMSG systems, and the thermal performance of the PMSG system shows more unequal distribution, where the difference of junction temperature between the IGBT and freewheeling diode is 12.4°C compared to 5.1°C in DFIG system. For the junction temperature of the grid-side converter, the thermal results of the DFIG and the PMSG systems are shown in Fig. 17(a) and Fig. 17(b), respectively. It can be seen that the hottest power semiconductor device turns out to be the IGBT. Moreover, the junction temperature variation between the IGBT and the diode show more equal distribution.

A further comparison of thermal behavior for both systems with different wind speed is shown in Fig. 18. For the generator-side converter, it can be seen that, in the PMSG system the mean junction temperature and the temperature fluctuation of the power semiconductors above rated wind speed are the highest all during the whole operation range of the wind. The hottest device is the diode in the whole wind speed range. In the DFIG system, the hottest device changes from the IGBT in the sub-synchronous mode to the diode in the super-synchronous mode. Moreover, the temperature fluctuation of the power semiconductors becomes crucial around synchronous operating point. Although the mean junction temperature is all higher in the PMSG system except for the region around synchronous operation as shown in upper Fig. 18(a), at rated wind speed the temperature fluctuation in the DFIG system is even larger due to less frequency power
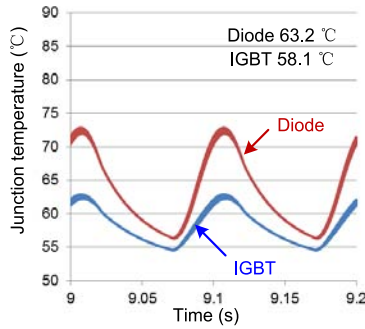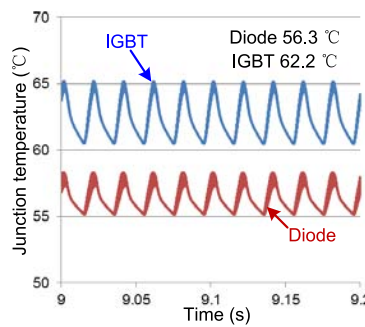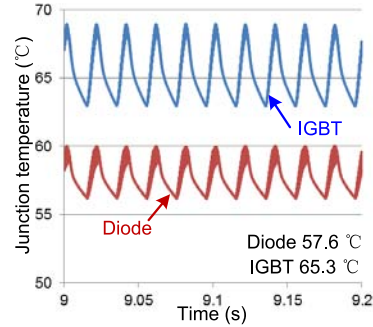

(a) DFIG system
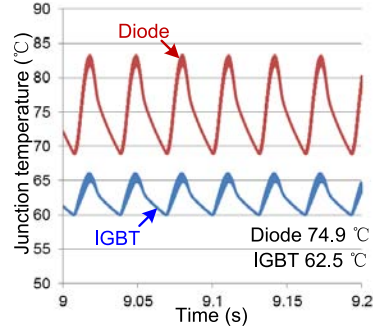
(b) PMSG system

Fig. 16. Junction temperature in the generator-side converter for the two wind turbine systems (Wind speed: 12 m/s)

(a) DFIG system

(b) PMSG system

Fig. 17. Junction temperature in the grid-side converter for the two wind turbine systems (Wind speed: 12 m/s)
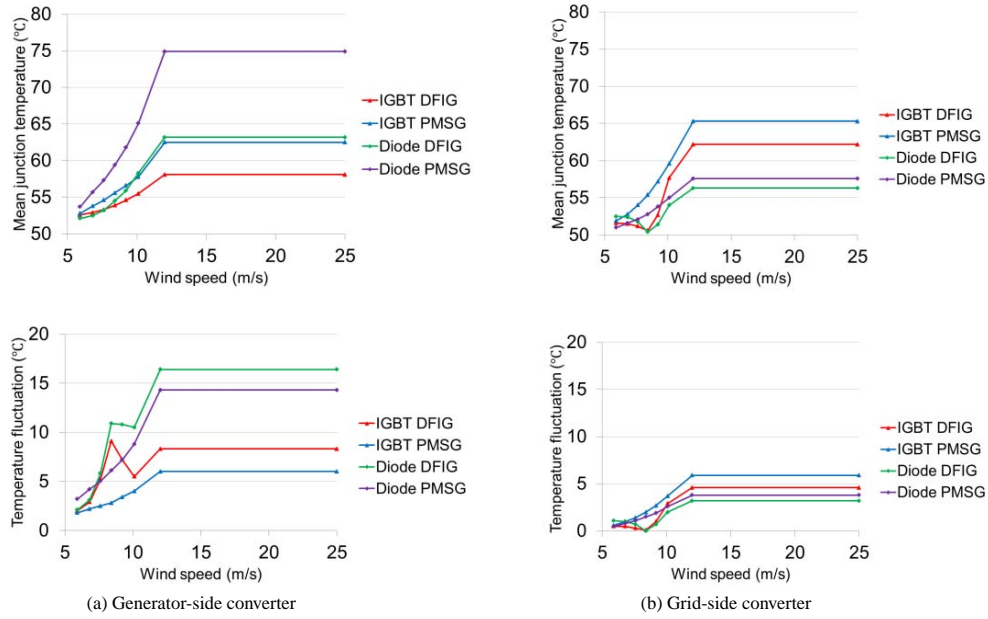
(a) Generator-side converter

(b) Grid-side converter

Fig. 18.   Mean junction temperature and temperature fluctuation in the chip vs. wind speed for both systems (unity power factor)

(a) Generator-side converter in the DFIG system
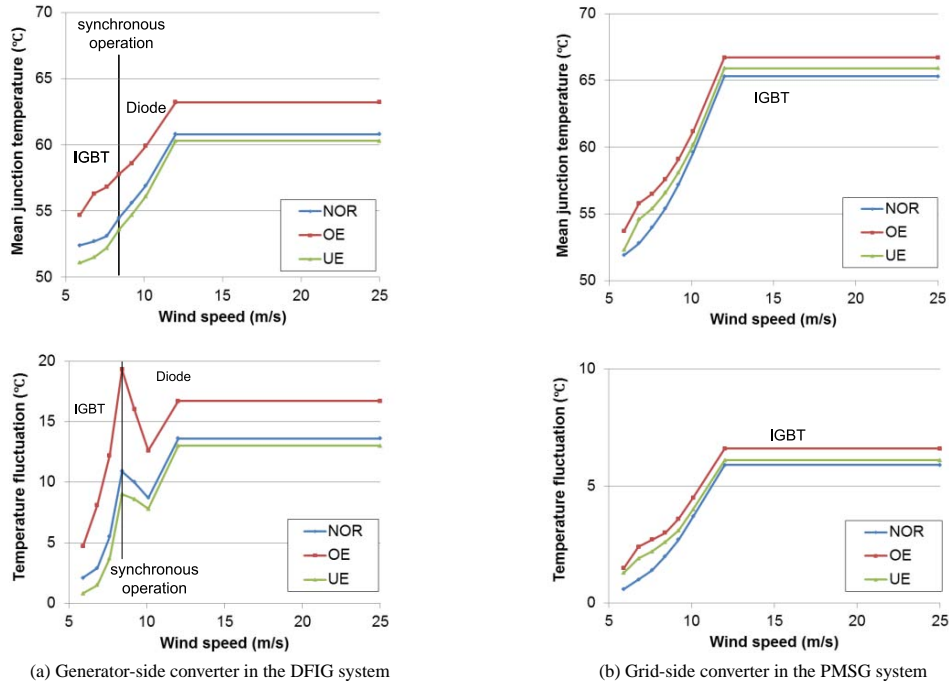
(b) Grid-side converter in the PMSG system

Fig. 19.   Thermal profile of the most stressed power semiconductor in the two different system considering grid codes. Note: NOR, OE and UE indicate normal, over-excited and under-excited reactive power, respectively

cycling as shown in lower Fig. 18(a).

5.3   Thermal Cycling Considering Grid Codes   As the most stressed power semiconductor decides the reliability and lifetime in a power module, it is necessary to extract the thermal excursion of the most serious loading chips in both the DFIG and PMSG system considering German grid codes shown in Fig. 8.

For the generator-side converter of the DFIG system as shown in Fig. 19(a), the most stressed power semiconductor changes from the IGBT in sub-synchronous mode to the freewheeling diode in super-synchronous mode. It is also noted

that the over-excited reactive power requirement will impose thermal stress to the power semiconductor especially at synchronous operating point. For the grid-side converter of the PMSG system, the IGBT is the most stressed power semiconductor during the whole operating wind speed. The reactive power injection will induce higher mean junction temperature and junction temperature fluctuation. Moreover, the situation will become worse at lower wind speed due to the lower output active power but the same amount of the reactive power is demanded.

6. Conclusion

In this paper, platforms for the popular 2 MW two-level wind turbine configurations (i.e. partial-scale and full-scale power converter) are established in the PLECS/Simulink to simulate the power losses and the thermal load cycling. A comparison of the loss distribution as well as thermal loading in the DFIG and the PMSG systems are investigated when considering the grid codes.

For the partial-scale power converter configuration, the thermal behavior between the generator-side converter and the grid-side converter are quite different. The operation area above the rated wind speed range of the grid-side converter is significant from the thermal stress point of view, while the generator-side converter not only concerns the above mentioned case, but also the wind speed range around the synchronous speed operation.

For the full-scale power converter configuration, whatever generator-side converter or grid-side converter, the crucial thermal stress lies in the operation area above the rated wind speed range.

Moreover, comparing the most stressed semiconductor device, the generator-side converter is the most critical part for thermal stress of the two-level back-to-back converter.

Furthermore, the reactive power support to the grid will affect the power loss profile and thermal profile of the power semiconductors, especially at lower wind speed.

References

(1) Z. Chen, J.M. Guerrero, and F. Blaabjerg: "A review of the state of the art of power electronics for wind turbines", *IEEE Trans. Power Electronics*, Vol.24, No.8, pp.1859–1875 (2009)

(2) F. Blaabjerg, Z. Chen, and S.B. Kjaer: "Power electronics as efficient interface in dispersed power generation systems", *IEEE Trans. Power Electronics*, Vol.19, No.5, pp.1184–1194 (2004)

(3) M. Liserre, R. Caárdenas, M. Molinas, and J. Rodriguez: "Overview of multi-MW wind turbines and wind parks", *IEEE Trans. Industrial Electronics*, Vol.58, No.4, pp.1081–1095 (2011)

(4) S. Faulstich, P. Lyding, B. Hahn, and P.J. Tavner: "Reliability of offshore turbines- identifying the risk by onshore experience", in Proc. of European Offshore Wind Energy Conference and Exposition (2009)

(5) B. Hahn, M. Durstewitz, and K. Rohrig: "Reliability of wind turbines- Experience of 15 years with 1500 WTs", Wind Energy: Proceedings of the Euromech Colloquium, pp.329–332, Springer-Verlag, Berlin.

(6) R. Johan and B.L. Margareta: "Survey of failures in wind power systems with focus on Swedish wind power plants during 1997–2005", *IEEE Trans. Energy Conversion*, Vol.22, No.1, pp.167–173 (2007)

(7) P.J. Tavner, J. Xiang, and F. Spinato: "Reliability analysis for wind turbines", Wind Energy, Vol.10, No.1, pp.1–18 (2007)

(8) ZVEL: Handbook for robustness validation of automotive electrical/electronic modules, Jun. (2008)

(9) Y. Song and B. Wang: "Survey on reliability of power electronic systems", *IEEE Trans. Power Electronics*, Vol.28, No.1, pp.591–604 (2013)

(10) A. Bryant, N. Parker-Allotey, D. Hamilton, I. Swan, P. Mawby, T. Ueta, T. Nishijima, and K. Hamada: "A fast loss and temperature simulation method for power converters, part I: eletrothermal modeling and validation", *IEEE Trans. Power Electronics*, Vol.27, No.1, pp.248–257 (2012)

(11) C. Busca, R. Teodorescu, F. Blaabjerg, S. Munk-Nielsen, L. Helle, T. Abeyasekera, and P. Rodriguez: "An overview of the reliability prediction related aspects of high power IGBTs in wind power applications", *Microelectronics Reliability*, Vol.51, No.9-11, pp.1903–1907 (2011)

(12) B. Lu and S. Sharma: "A literature review of IGBT fault diagnostic and protection methods for power inverters", *IEEE Trans. Industry Applications*, Vol.45, No.5, pp.1770–1777 (2009)

(13) D. Hirschmann, D. Tissen, S. Schroder, and R.W. De Doncker: "Reliability prediction for inverters in hybrid eletrical vehicles", *IEEE Trans. Power*

Electronics, Vol.22, No.6, pp.2511–2517 (2007)

(14) N. Kaminski: "Load-cycle capability of HiPaks", ABB Application Note 5SYA 2043-01 (2004)

(15) O.S. Senturk, L. Helle, S. Munk-Nielsen, P. Rodriguez, and R. Teodorescu: "Power capability investigation based on electrothermal models of press-pack IGBT three-level NPC and ANPC VSCs for multi-MW wind turbines", *IEEE Trans. on Power Electronics*, Vol.27, No.7, pp.3195–3206 (2012)

(16) H. Wang, K. Ma, and F. Blaabjerg: "Design for reliability of power electronic systems", in Proc. of IECON 2012, pp.33–44 (2012)

(17) F. Blaabjerg, K. Ma, and D. Zhou: "Power Electronics and Reliability in Renewable Energy Systems", in Proc. of ISIE 2012, pp.20–30 (2012)

(18) Y. Avenas, L. Dupont, and Z. Khatir: "Temperature measurement of power semiconductor devices by thermo-sensitive electrical parameters—a review", *IEEE Trans. Power Electronics*, Vol.27, No.6, pp.3081–3092 (2012)

(19) W. Lixiang, J. McGuire, and R.A. Lukaszewski: "Analysis of PWM frequency control to improve the lifetime of PWM inverter", *IEEE Trans. Industry Applications*, Vol.47, No.2, pp.922–929 (2011)

(20) A. Wintrich, U. Nicolai, and T. Reimann: "Semikron Application Manual", p.128 (2011)

(21) F. Blaabjerg, M. Liserre, and K. Ma: "Power electronics converters for wind turbine systems", *IEEE Trans. Industry Applications*, Vol.48, No.2, pp.708–719 (2012)

(22) M. Chinchilla, S. Arnaltes, and J.C. Burgos: "Control of permanent-magnet generators applied to variable-speed wind-energy systems connected to the grid", *IEEE Trans. Energy Conversion*, Vol.21, No.1, pp.130–135 (2006)

(23) "Vestas". [Online]. Available: http://www.vestas.com/

(24) A.A. Rockhill, M. Liserre, R. Teodorescu, and P. Rodriguez: "Grid-filter design for a multi-megawatt medium-voltage voltage-source inverter", *IEEE Trans. on Industrial Electronics*, Vol.58, No.4, pp.1205–1217 (2011)

(25) M. Chinchilla, S. Arnaltes, and J.C. Burgos: "Control of permanent-magnet generators applied to variable-speed wind-energy systems connected to the grid", *IEEE Trans. Energy Conversion*, Vol.21, No.1, pp.130–135 (2006)

(26) C. Liu, F. Blaabjerg, W. Chen, and D. Xu: "Stator current harmonic control with resonant controller for doubly fed induction generator", *IEEE Trans. Power Electronics*, Vol.27, No.7, pp.3207–3220 (2012)

(27) H. Li, Z. Chen, and H. Polinder: "Optimization of multibrid permanent-magnet wind generator systems", *IEEE Trans. Energy Conversion*, Vol.24, No.1, pp.82–92 (2009)

(28) M. Altin, O. Goksu, R. Teodorescu, P. Rodriguez, B. Bak-Jensen, and L. Helle: "Overview of recent grid codes for wind power integration", in Proc. of OPTIM'2010, pp.1152–1160 (2010)

(29) M. Tsili and S. Papathanassiou: "A review of grid code technical requirements for wind farms", *IET Renewable Power Generation*, Vol.3, No.3, pp.308–332 (2009)

(30) E.ON-Netz. Requirements for offshore grid connections (2008)

(31) B. Backlund, R. Schnell, U. Schlapbach, R. Fischer, and E. Tsyplakov: "Applying IGBTs" (2011)

(32) User manual of PLECS blockset version 3.2.7 March 2011. (Available: http://www.plexim.com/files/plecsmanual.pdf)

(33) J. Jung and W. Hofmann: "Investigation of thermal stress in rotor of doubly-fed induction generator at synchronous operating point", in Proc. of IEMDC 2011, pp.896–901 (2011)

(34) S. Engelhardt, I. Erlich, C. Feltes, J. Kretschmann, and F. Shewarega: "Ractive power capability in wind turbines based on doubly fed induction generators", *IEEE Trans. Energy Conversion*, Vol.26, No.1, pp.364–372 (2011)

(35) K. Ma and F. Blaabjerg: "Multilevel converters for 10 MW wind turbines", in Proc. of EPE 2011, pp.1–10 (2011)

(36) D. Zhou, F. Blaabjerg, M. Lau, and M. Tonnes: "Thermal analysis of multi-MW two-level wind power converter", in Proc. of IECON 2012, pp.5862–5868 (2012)

Dao Zhou (Non-member) received the B.Sc. in electrical engineering from Beijing Jiaotong University, Beijing, China, in 2007, and the M.Sc. in power electronics from Zhejiang University, Hangzhou, China, in 2010. From 2012, he is pursuing the Ph.D degree in the Department of Energy Technology, Aalborg University, Aalborg, Denmark. His research interests include two-level power electronics converters and their application in wind power generation systems.
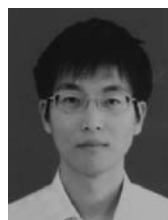
Frede Blaabjerg (Non-member)　received the M.Sc.EE. and Ph.D degrees from Aalborg University, Aalborg East, Denmark in 1987 and 1995, respectively. He was employed at ABB-Scandia, Randers, from 1987–1988. During 1988–1992 he was PhD. student at Aalborg University, Denmark, became Assistant Professor in 1992, Associate Professor in 1996 and full professor in power electronics and drives in 1998. He has been part-time research leader at Research Center Risoe in wind turbines. In 2006–2010 he was dean of the faculty of Engineering, Science and Medicine and became visiting professor at Zhejiang University, China in 2009. His research areas are in power electronics and its applications like wind turbines, PV systems and adjustable speed drives. Since 2006 he has been Editor in Chief of the IEEE Transactions on Power Electronics. He was Distingueshed lecturer for the IEEE Power Electronics Society 2005–2007 and for IEEE Industry Applications Society from 2010–2011. Dr. Blaabjerg received the 1995 Angelos Award for his contribution in modulation technique and the Annual Teacher prize at Aalborg University. In 1998 he received the Outstanding Young Power Electronics Engineer Award from the IEEE Power Electronics Society. He has received ten IEEE Prize paper awards and another prize paper award at PELINCEC Poland 2005. He received the IEEE PELS Distingueshed Service Award in 2009 and the EPE-PEMC 2010 Council award.

Mogens Lau (Non-member)　received the M.Sc. in Electrical engineering from Aalborg University, Aalborg, Denmark, in 1999. He worked as development engineer, project manager and line manager within power electronics at leading companies like Danfoss, Grundfoss and Vestas. Currently he is the R&D manager of Danfoss power stacks at Danfoss Silicon Power GmbH.

Michael Tonnes (Non-member)　received the Ph.D in electrical engineering from Aalborg University, Aalborg, Denmark. Currently he is the senior director of Danfoss power stacks at Danfoss Silicon Power GmbH.